Optimisation of mapping modes for heterodyne instruments

V. Ossenkopf

SRON National Institute for Space Research,
P.O. Box 800, 9700 AV Groningen,
Netherlands

March 11, 2004

Abstract

Line mapping with single-pixel heterodyne instruments is usually performed either in an On-The-Fly (OTF) or in a raster mapping mode depending on the capabilities of the telescope and the instrument. In general the observing efficiency can be increased by combining several source point integrations with a common reference measurement. This is already implemented at many telescopes, however, a thorough investigation of the optimum calibration of the modes and the best way of performing these observations is still lacking.

Here, we use the knowledge on the system stability obtained by an Allan variance measurement to derive general rules and a mathematical formalism for optimising the setup of mapping observations. Special attention has to be paid to the minimisation of the impact of correlated noise introduced by the common OFF integrations and to the correction of instrumental drifts. Both aspects can be covered by using a calibration scheme that interpolates between two OFF measurements taken with an integration time that is $0.7\sqrt{N}$ times the integration time for each of the N source points between the two OFF measurements.

The total uncertainty of the calibrated data consisting of radiometric noise and drift noise can be minimised by adjusting the source integration time and the scan length N. It turns out that OTF observations are very robust providing a low relative noise even if their setup deviates considerably from the optimum. Fast data readouts are often essential to minimise the drift contributions, but for continuum observations they will nevertheless exceed in many cases the radiometric noise leading to a very poor overall data quality.

The main drawback of the described mapping modes is the limited use of the measured data with respect to a later spatial or spectroscopic rebinning.

Contents

1 Introduction

Schieder & Kramer (2001) showed that the knowledge on the system stability of a heterodyne instrument can be used to obtain optimum parameters for performing actual observations with the instrument. They computed the timing parameters providing the minimum uncertainty of the calibrated data, consisting of radiometric noise and drift noise, per unit of observing time for two basic observing modes. Unfortunately, their computations were restricted to fluctuations with an $1/f^{\alpha}$ power spectrum with a spectral index α between 2 and 3. This spectral index is representative for spectroscopic fluctuations across a given backend (Ossenkopf 2003), but recent measurements by Whyborn (2003) have shown that fluctuations of the total power level of the signal typically follow a much shallower spectral index of about 0.7. This requires a revision of their results with respect to generalising the spectral index.

Moreover, Schieder & Kramer (2001) assumed a special calibration scheme for all mapping modes where single rows in a map are combined with a single reference measurement for calibration, although other calibration schemes are possible as well. Thus we have repeated their computations in a more general framework allowing for various calibration schemes and arbitrary spectral indices resulting in general guidelines for an optimum performance and calibration of mapping observations.

As corresponding optimisations for observing modes with single source and reference positions, including position switch, chop, and frequency switch modes, were already introduced by Ossenkopf (2003), we restrict ourselves here to mapping observing modes. Depending on the capabilities of the telescope and the instrument, mapping can be performed either in an On-The-Fly (OTF) or in a raster mapping mode. Beuther et al. (2000) has shown that OTF modes are in principle always preferable from the viewpoint of the observing efficiency. They impose, however, harder requirements to the pointing and timing behaviour of the telescope, which may not always be given. Because the delay between adjacent points in the raster mapping adds only a small complication to the optimisation problem we will concentrate here on the OTF mapping discussing the deviations from this mode for raster maps only in the Appendix.

The outline of the paper follows our basic approach to the optimisation problem. In Sect. 2 we introduce the properties of the mapping modes and discuss the possible ways how the measured data will be calibrated to obtain scientific data. In Sect. 3 we evaluate the different calibration schemes with respect to their sensitivity to drift effects. In Sect. 4 we demonstrate the application of the different calibration schemes to actual observations performed at the KOSMA 3 m telescope. Choosing the best calibration scheme we then optimise the exact timing of the observations with respect to radiometric noise and drift noise in Sect. 5. The conclusions for the observing mode efficiencies are summarised in Sect. 6.

2 Introduction to OTF observations

2.1 The general measurement scheme

A general introduction to OTF mapping was given by Beuther et al. (2000). OTF mapping with a position switch reference is the most efficient – and thus frequently applied

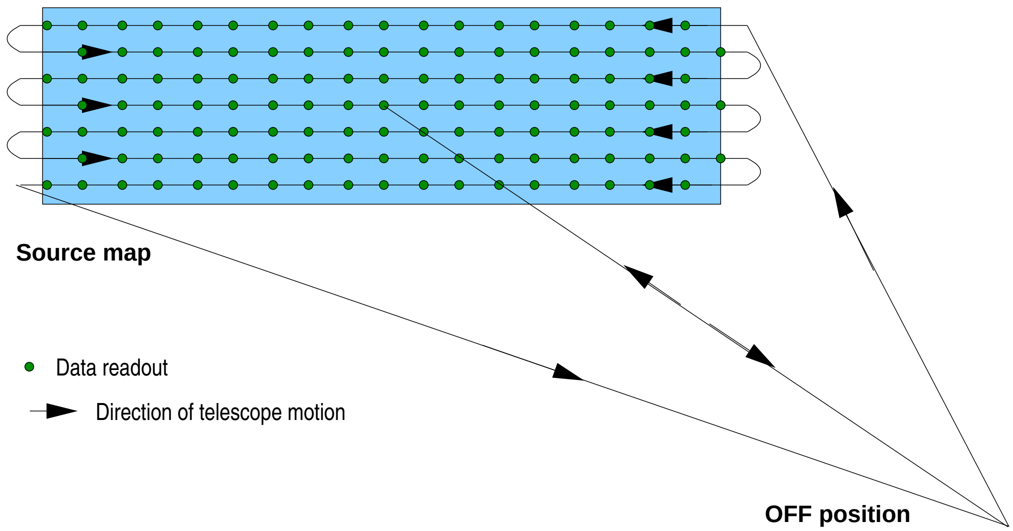

Figure 1: Demonstration of the general properties of an OTF observation. In this example, the OFF position is visited twice within one coverage of the whole map. An additional OFF measurement is performed at the end of the observation. The green dots symbolise the points where the backends are read out. The integration starts when the telescope enters the blue area of the map. In this example, the scanning direction is changed after each row.

– mode for the observation of large fields in the sky with single-pixel receivers. The gain in the observing efficiency relative to other observing modes stems both from the lack of dead times between the observation of adjacent points and from the reuse of the observation of a single reference position for the calibration of several data points. The general sequence of operations is demonstrated in Fig. 1. This example corresponds to a mode implemented for the Herschel satellite, where a turn is performed between subsequent lines so that they are scanned in opposite directions. Moreover, it is possible here to go from an arbitrary position within the map to the reference position whereas the implementation of the OTF mode at most ground-based telescopes foresees an OFF measurement after each full scan line. We will consider the most general case here.

The instrument integrates here for the full time between two data read-outs, symbolised by the green dots in the picture. This leads to smearing, i.e. broadening of the effective beam characterising the measurement along the scanning direction. Beuther et al. (2000) have shown that for OTF maps where the readout is performed on a spatial grid corresponding to a Nyquist sampling of the map with the beam profile, the effective beam broadening is less than 4 %. An edge taper of 14 dB was assumed there.

However, we can foresee a number of observations which will not be performed exactly on Nyquist sampling. Traditionally the difference between a sampling at half the beam width, FPBW/2, and a full Nyquist sampling with FPBW/2.4 (for a 14 dB edge taper) is ignored by using the slightly coarser sampling. This can be justified by the drop of the relative gain of information on the spatial structure of an object per observing time when using a finer sampling below the beam size (Bensch et al. 2001). Moreover, the huge frequency coverage of the HIFI instrument will allow a mapping of the same astronomical object in different frequencies with different beam widths. Here, it is obviously impossible to observe exactly the same area with a Nyquist sampling at all frequencies. Thus compromises will be made resulting in samplings deviating from a full Nyquist sampling.

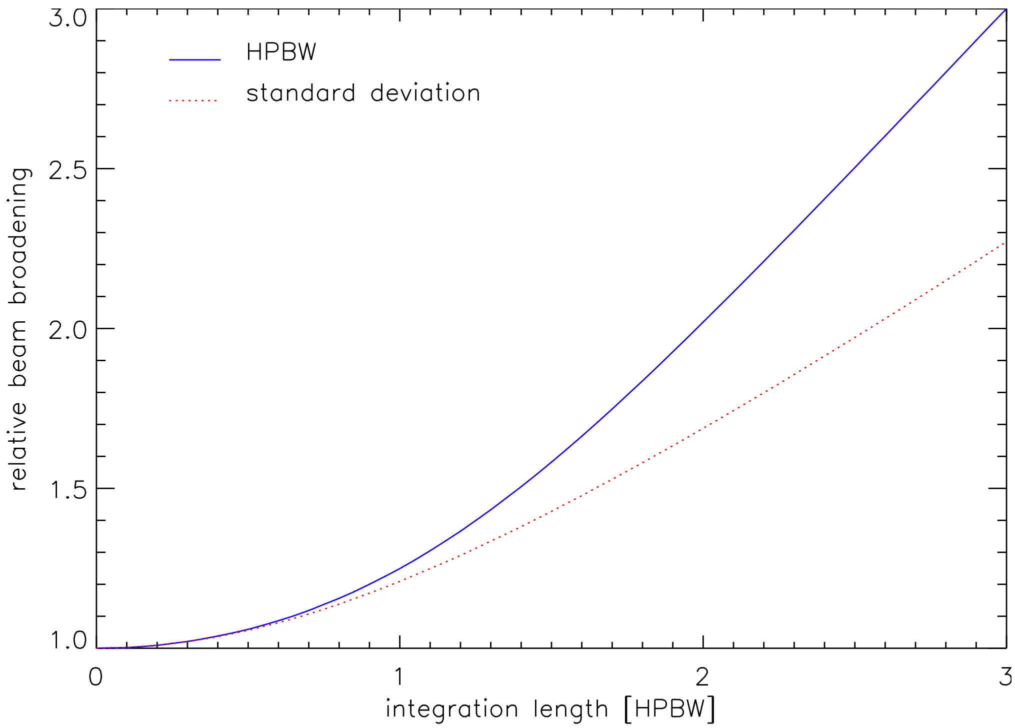

Figure 2: Beam broadening due to the scanning motion of the telescope during integration in OTF observations. The solid line shows the ratio between the HPBW of the effective beam in scanning direction and the original Gaussian beam. The dotted line represents the ratio between the corresponding standard deviations.

We can compute the quantitative impact of the beam smearing in the general case by the numerical convolution of a two-dimensional Gaussian beam profile with a strip function of finite size representing the motion of the telescope during the integration. The result is shown in Fig. 2. The solid line shows the increase of the half-power beam width (HPBW) with increased scanning length. We find that the beam broadening goes from the mentioned 4 % at the Nyquist sampling of 0.42 HPBW to 6 % at 0.5 HPBW and to 25 % at 1 HPBW. When using a scanning length above 2 HPBW, the beam is completely dominated by the strip length. Already at 2 HPBW, the original beam contributes only by 2 %. This is also visible in the beam shape. To judge the beam shape we have plotted the ratio between the standard deviation of the actual beam and the original beam as dotted line. The difference between the two curves gives a measure for the degree of "non-Gaussianity" of the beam. The beam shape is close to Gaussian for scan lengths below 1 HPBW and almost rectangular above 2 HPBW. The beam size perpendicular to the scanning direction is not influenced by the scans.

Thus the OTF mode does not provide a noticeable beam broadening as long as the data readout is performed on a time scale corresponding to a telescope motion of less than about 0.65 HPBW. When observations ask for a lower resolution than actually provided by the beam. e.g. for the comparison of line ratios, or a coarser sampling, it is possible to integrate longer thus reducing the noise. With integration times corresponding to more than about 1.8 HPBW the actual measurement then represents a rectangular profile along the scanning direction. Nevertheless, even in these cases the data should be read out faster (with approximately the Nyquist sampling) to allow a possible further analysis of the data with the full resolution of the telescope.

2.2 The calibration by a reference measurement

All astronomical measurements suffer in principle from temporal drifts of the instrumental sensitivity which can lead to inaccurately calibrated data. Heterodyne measurements use the regular observation of a reference to correct for the drift effects. The mapping modes considered here, use a point on the sky which is free of emission, the OFF position, as reference. The calibrated data are then obtained by subtracting the count rate on the OFF from the count rate on the source (Kutner & Ulich 1981, Ossenkopf 2002).

Consequently the radiometric noise in the calibrated data for each pixel consists of noise contributions from the source integrations and from the OFF measurement, $\sigma_{\rm noise} \propto \sqrt{1/t_{\rm s} + 1/t_{\rm OFF}}$. In case of the lack of any dead times it can be easily shown that the radiometric noise is minimised when using an OFF integration time $t_{\rm OFF} = \sqrt{N} t_{\rm s}$, if N source integrations with $t_{\rm s}$ are calibrated with the same OFF measurement (Ball 1976). Although this relation is not strictly fulfilled in the situation of non-negligible overheads, it is still approximately given there (Schieder & Kramer 2001) and thus widely used in current implementations of OTF observing modes at ground-based telescopes.

There are three different calibration approaches in common use:

i) single OFF: The reference position is observed for $t_{\rm R} = t_{\rm OFF}$ before (or after) a series of N source points and the count rate there is subtracted from all source points in the series.

$$C_{{\rm s},i} = c_{{\rm s},i} - c_{\rm R} \tag{1}$$

where the index i running from 1 to N characterises the different source points in a series. This approach is currently used as standard calibration for OTF observations at the JCMT and at KOSMA.

ii) interpolated OFF: The total OFF integration time $t_{\rm OFF}$ is split into two OFF observations with half the integration time, $t_{\rm R} = t_{\rm OFF}/2$, before and after the series of N source points. The reference count rate subtracted from each source count rate is given by the linear interpolation between the two OFF measurements

$$C_{{\rm s},i} = c_{{\rm s},i} - [(1-l)c_{{\rm R},1} + l c_{{\rm R},2}] \tag{2}$$

Here, l is given by a time interpolation equation which results in $l = 0$ if the source count rate is measured at the time of the first OFF observation and in $l = 1$ if it is measured at the time of the second OFF. It can be obtained from

$$l = \frac{t_{\rm R}/2 + t_{\rm d,1} + (i - 1/2)t_{\rm s}}{t_{\rm R} + t_{\rm d,1} + t_{\rm d,2} + N t_{\rm s}} \tag{3}$$

where the terms $t_{\rm d,1}$ and $t_{\rm d,2}$ stand for the dead times when going from the OFF position to the first source point and from the last source point to the OFF position. The number i denotes the index of the source point in the current scan and N is the total number of source points between two OFF measurements.

The actual timing for the observation can be almost identical to case **i)** because the OFF measurements between the source series are simply split into two subsequent OFF measurements with the half time. The only difference is that the whole observation is bracketed between two OFF measurements with half the standard OFF integration time. This approach is currently the default setting for the OTF calibration at the IRAM 30 m telescope.

iii) double OFF: This approach uses the same splitting of the OFF measurement into two parts before and after the source series as case **ii)** but uses the average of both count rates for the calibration instead of applying a linear interpolation in time.

$$C_{\mathrm{s},i} = c_{\mathrm{s},i} - \left[\frac{1}{2} c_{\mathrm{R},1} + \frac{1}{2} c_{\mathrm{R},2}\right] \quad (4)$$

It corresponds to Eq. (2) with a fixed value $l = 0.5$.

This approach guarantees that all source points in a series are calibrated with the same OFF count rate corresponding to the value obtained in the linear interpolation at the centre of the series of source points.

The obvious advantage of the linear interpolation (**ii**) is the complete cancellation of all linear drifts. The disadvantage is the production of a varying noise across each series of source points resulting from the variable OFF contributions. In the centre of each series, where $l = 0.5$, the noise from the OFF position corresponds to an integration time of t_{OFF}, but at the ends, where $l = 0$ or $l = 1$, the noise from the OFF is higher by $\sqrt{2}$ because only a single measurement with $t_{\mathrm{R}} = t_{\mathrm{OFF}}/2$ contributes there. This is actually visible in some IRAM observations where the noise is minimal in the centre of each line but increasing towards the edges of the maps (Teyssier, priv.comm.). However, the effect is relatively small because the noise contribution from the OFF integration to the total noise is small for large scans, when $t_{\mathrm{OFF}} = \sqrt{N} t_{\mathrm{s}}$ is used, so that its change by a factor of $\sqrt{2}$ does not have a big impact on the overall calibration.

2.3 Correlated noise

The calibration of the data from several source points with a common OFF measurement always produces a certain amount of correlated noise in the final data. Because the different reference calibration approaches imply different ways of adding the noise from the neighbouring two OFF measurements to a series of source data they will result in a different amount of correlated noise throughout any OTF map. When the calibration involves a temporal interpolation, the correlated noise will also vary from point to point.

Because of this temporal dependence there is no unique single parameter to quantify the correlated noise, but several ways are possible. To avoid a complex multidimensional description we will nevertheless use here a simple parameter for the correlated noise given by the product of the number of pixels showing the same noise contribution and the variance of this noise. This definition reflects a measure for the visual effect of correlated noise in a map where the eye automatically integrates over parts of the map to detect structures. The product of the variance with the pixel number then corresponds to this integration.

For the comparison of the correlated noise between the different OFF calibration schemes we use the single-OFF calibration as a reference. The correlated noise behaviour

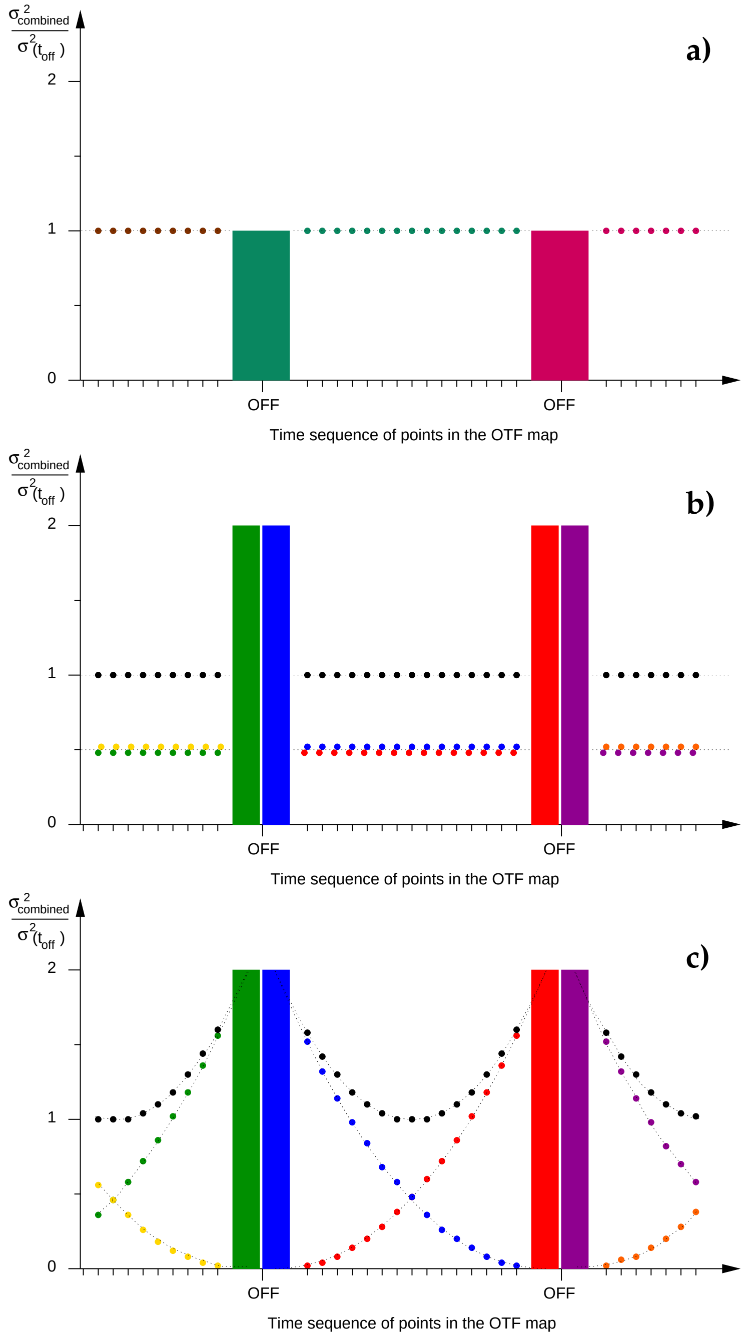

Figure 3: Demonstration of the correlated noise across the source spectra produced by the subtraction of the reference measurements for the different calibration schemes discussed in Sect. 2.2. The coloured bars in the time series indicate OFF measurements. Their height represents the noise in the OFF measurement corresponding to the integration time. The coloured dots indicate the correlated noise contribution from the OFF measurement with the corresponding colour to the calibrated source data. The black dots stand for the total noise variance added from the reference measurements to each source data point. Part **a** represents the single OFF calibration, part **b** the double-OFF calibration, and part **c** the interpolated-OFF calibration.

for this scheme is visualised in Fig. 3a. The coloured bars in the time series represent the different OFF measurements and the dots with the corresponding colour indicate the relative contribution of the noise from the corresponding OFF measurement to the calibrated source data. The correlated noise is given here by the sum of the height of all dots between two subsequent OFF measurements.

The situation for the double-OFF calibration is demonstrated in Fig. 3b. When splitting the OFF measurement between two OTF scans into two parts the absolute noise variance in each of these parts is twice the noise of the original measurement. When calibrating the source data with the fixed ratio $l = 1/2$ each source point "feels" only half of the noise variance from each of the OFF measurements, indicated by the coloured dots, compared to the single-OFF calibration. The sum of their uncorrelated contributions then provides a noise level identical to the single-OFF treatment. The correlated noise from each OFF measurement, however, is only half the value from the single-OFF calibration. Hence, the somewhat better treatment of instrumental drifts by the double-OFF calibration is also accompanied by a reduction of the correlated noise, so that this method is clearly superior to the single-OFF calibration.

Fig. 3c shows the behaviour for a linearly interpolated-OFF calibration

With the linear interpolation between the two adjacent OFF measurements, we obtain the increased total noise close to the boundaries of each scan as discussed above. The total noise variance varies between the value for the single-OFF calibration at the scan centre and twice this values at the boundaries. The correlated noise from each OFF measurement varies strongly across a scan. An upper limit to the correlated noise sum from one OFF measurement can be obtained when neglecting the finite integration time for the OFF measurement and replacing the sum by an integral. This integral amounts to 2/3 of the correlated noise sum obtained in the single-OFF calibration. For the total noise, the integral would, however, show 4/3 of the value for the single-OFF calibration. Thus, the linear interpolation shows a slightly increased total noise but a decreased correlated noise contribution compared to the single-OFF scheme. However, the double-OFF calibration is clearly superior in both aspects.

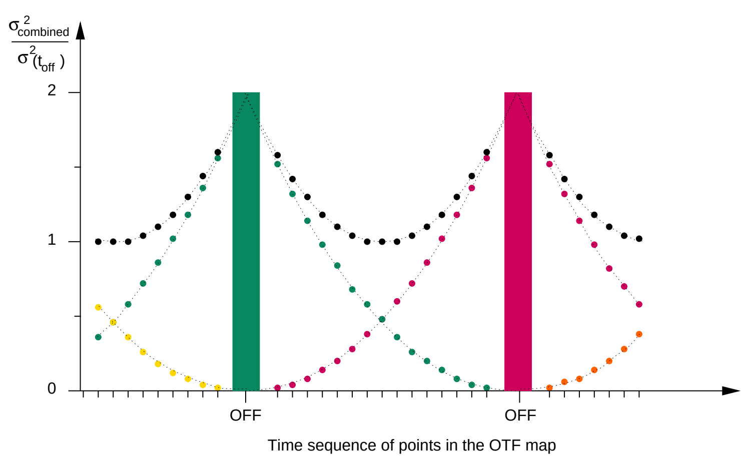

Figure 4: Demonstration of the correlated noise for an interpolated OFF calibration where the OFF measurement is used for both adjacent source scans and the OFF integration time is half of the integration time used in the schemes shown in Fig. 3.

An obvious further step towards an increase of the efficiency of the observations is the reuse of an OFF measurement for two two adjacent scans so that the OFF integration time can be reduced by a factor two. When using the full OFF integration time for the reference time, i.e. $t_\mathrm{R} = t_\mathrm{OFF}$, all the equations from Sect. 2.2 are still valid. For the interpolated-OFF calibration this is demonstrated in Fig. 4. Beside the efficiency gain due to the reduction of the OFF integration time we find that the correlated noise is increased now by a factor two because the noise from one OFF measurement is spread across the two adjacent scans. The total noise variance sum, however, does not differ from Fig. 3.

In case of the double-OFF calibration both the total noise variance and the correlated noise sum are now identical to the values in the single-OFF calibration with twice the OFF integration time. For the interpolated OFF calibration both the correlated noise and the total noise variances are now higher by a factor of up to 4/3 than the value obtained in the single-OFF calibration. Vice versa we can use an OFF calibration time of 2/3 of the time used in the single-OFF calibration to obtain the same amount of total noise and correlated noise in the interpolated-OFF calibration.

Thus we find three different ways to produce the same total noise contribution and the same degree of correlation in the noise from the OFF measurement to each source measurement. The single-OFF calibration uses each OFF integration time for a full scan containing no drift corrections at all. In the double-OFF calibration we can reduce the OFF integration time to 1/2 and obtain in addition a reduction of the drift error by at least a factor two. In the interpolated-OFF calibration we need an OFF integration time of 2/3 compared to the single-OFF calibration but obtain a complete cancellation of all linear drift errors.

After these general considerations we will actually compute the error in the calibrated data due to both instrumental drift and the radiometric noise both from the source points and from the OFF subtraction in the next section.

3 Computation of the data uncertainty due to noise and drift

3.1 General quantification of the noise and drift fluctuations

The total uncertainty of the measured data composed of radiometric noise and drift noise can be computed from the statistics of both fluctuation spectra. This has been performed by Schieder & Kramer (2001) using special assumptions on the implementation of the OTF mode and on the fluctuation spectra. Here, we repeat these computations for the general case.

If the measured signal is described by a continuous function $s(t)$ the difference between the count rate for a source measurement and the corresponding OFF measurement can be written as

$$\begin{aligned} C_{\mathrm{s},i} &= c_{\mathrm{s},i}(t) - (1-l)c_{\mathrm{R},1}(t) - l c_{\mathrm{R},2}(t) \\ &= \frac{1}{t_\mathrm{s}} \int_{t+t_\mathrm{R}+t_{\mathrm{D},1}}^{t+t_\mathrm{R}+t_{\mathrm{D},1}+t_\mathrm{s}} dt'\, s(t') \end{aligned} \tag{5}$$

$$
\begin{aligned}
&-(1-l)\frac{1}{t_{\mathrm{R}}}\int_{t}^{t+t_{\mathrm{R}}} dt'\ s(t') \\
&-l\frac{1}{t_{\mathrm{R}}}\int_{t+t_{\mathrm{scan}}+t_{\mathrm{R}}}^{t+t_{\mathrm{scan}}+2t_{\mathrm{R}}} dt'\ s(t')
\end{aligned} \tag{6}
$$

To abbreviate the notation we use here the total delay time before a given source measurement i, $t_{\mathrm{D},1} = t_{\mathrm{d},1} + (i-1)t_{\mathrm{s}}$ and the time between two OFF measurements, $t_{\mathrm{scan}} = t_{\mathrm{d},1} + Nt_{\mathrm{s}} + t_{\mathrm{d},2}$. This equation can be used for all calibration schemes discussed above when using the general weighting factors l and $1-l$. For the case of the single OFF l is simply set to 1 or 0 and for the double OFF $l = 1/2$. In all cases where the OFF measurement is split into two separate contributions we use $t_{\mathrm{R}} = t_{\mathrm{OFF}}/2$, otherwise $t_{\mathrm{R}} = t_{\mathrm{OFF}}$.

The average total uncertainty of the count rate is then

$$
\sigma_C^2(i) = \left\langle (C_{\mathrm{s},i} - \langle C_{\mathrm{s},i}\rangle_t)^2 \right\rangle_t \tag{7}
$$

where we treat the measurement as a continuous function, ignoring that it can be performed only in discrete steps.

It can be easily seen that the maximum uncertainty occurs for weak signals where the count rates on the source and on the OFF position are almost the same. Thus we start here with this worst case assuming $\langle c_{\mathrm{s},i}(t) - (1-l)c_{\mathrm{R},1}(t) - lc_{\mathrm{R},2}(t)\rangle_t = 0$. Then the second term in Eq. (7) vanishes and we can rewrite it as

$$
\begin{aligned}
\sigma_C^2(i) \;=\; & \left\langle c_{\mathrm{s},i}(t)^2\right\rangle_t + (1-l)^2 \left\langle c_{\mathrm{R},1}(t)^2\right\rangle_t + l^2 \left\langle c_{\mathrm{R},2}(t)^2\right\rangle_t \\
& -2(1-l)\left\langle c_{\mathrm{s},i}(t)c_{\mathrm{R},1}(t)\right\rangle_t - 2l\left\langle c_{\mathrm{s},i}(t)c_{\mathrm{R},2}(t)\right\rangle_t \\
& +2l(1-l)\left\langle c_{\mathrm{R},1}(t)c_{\mathrm{R},2}(t)\right\rangle_t
\end{aligned} \tag{8}
$$

The first three contributions contain the variation representing the noise within each of the three measurements involved. The other terms represent the cross correlation between them containing all drift terms.

The computation scheme for all six terms follows the same approach. We demonstrate it here only for $\langle c_{\mathrm{s},i}(t)c_{\mathrm{R},1}(t)\rangle_t$:

$$
\langle c_{\mathrm{s},i}(t)c_{\mathrm{R},1}(t)\rangle_t = \left\langle \frac{1}{t_{\mathrm{s}}t_{\mathrm{R}}}\int_t^{t+t_{\mathrm{R}}} dt' \int_{t+t_{\mathrm{R}}+t_{\mathrm{D},1}}^{t+t_{\mathrm{R}}+t_{\mathrm{D},1}+t_{\mathrm{s}}} dt''\ s(t')s(t'') \right\rangle_t \tag{9}
$$

With an appropriate coordinate transformation to time variables τ' and τ'' starting at the beginning of the two involved measurements we obtain

$$
\langle c_{\mathrm{s},i}(t)c_{\mathrm{R},1}(t)\rangle_t = \left\langle \frac{1}{t_{\mathrm{s}}t_{\mathrm{R}}}\int_0^{t_{\mathrm{R}}} d\tau' \int_0^{t_{\mathrm{s}}} d\tau''\ s(t-\tau')s(t-\tau''+t_{\mathrm{D},1}+t_{\mathrm{s}}) \right\rangle_t \tag{10}
$$

The integrals can be evaluated if we know the auto-correlation function of the fluctuation spectrum. For a power-law noise spectrum $S(f) \propto 1/f^{\alpha}$ with spectral indices α between 0 and 3[1] the auto-correlation function can be evaluated as

$$
\begin{aligned}
\gamma(\tau) &= \langle s(t+\tau)s(t)\rangle_t \\
&= g_0 - g_\alpha \tau^{\alpha-1}
\end{aligned} \tag{11}
$$

[1]There exists a logarithmic deviation for $\alpha = 1$, so that equation does not hold for this particular value.

assuming zero averages (Schieder & Kramer 2001).

Exploiting this relation we can exchange the sequence of integration and averaging resulting in

$$
\begin{aligned}
\langle c_{\mathrm{s},i}(t) c_{\mathrm{R},1}(t)\rangle_t &= \frac{1}{t_\mathrm{s} t_\mathrm{R}} \int_0^{t_\mathrm{R}} d\tau' \int_0^{t_\mathrm{s}} d\tau'' \gamma(\tau' - \tau'' + t_{\mathrm{D},1} + t_\mathrm{s}) \\
&= g_0 - \frac{g_\alpha}{\alpha(\alpha+1) t_\mathrm{s} t_\mathrm{R}} \left\{ [t_{\mathrm{D},1} + t_\mathrm{s} + t_\mathrm{R}]^{\alpha+1} - [t_{\mathrm{D},1} + t_\mathrm{R}]^{\alpha+1} \right. \\
&\qquad \left. - [t_{\mathrm{D},1} + t_\mathrm{s}]^{\alpha+1} + t_{\mathrm{D},1}^{\alpha+1} \right\}
\end{aligned} \tag{12}
$$

Applying the same procedure to all terms in Eq. (8) results in

$$
\begin{aligned}
\sigma_\mathrm{C}^2(i) &= \frac{-2 g_\alpha}{\alpha(\alpha+1)} \left\{ t_\mathrm{s}^{\alpha-1} + (1 - 2l + 2l^2) t_\mathrm{R}^{\alpha-1} \right. \\
&\quad + l(1-l) \frac{(2t_\mathrm{R} + t_\mathrm{scan})^{\alpha+1} - 2(t_\mathrm{R} + t_\mathrm{scan})^{\alpha+1} + t_\mathrm{scan}^{\alpha+1}}{t_\mathrm{R}^2} \\
&\quad - (1-l) \frac{(t_\mathrm{R} + t_{\mathrm{D},1} + t_\mathrm{s})^{\alpha+1} - (t_\mathrm{R} + t_{\mathrm{D},1})^{\alpha+1} - (t_{\mathrm{D},1} + t_\mathrm{s})^{\alpha+1} + t_{\mathrm{D},1}^{\alpha+1}}{t_\mathrm{R} t_\mathrm{s}} \\
&\quad \left. - l \frac{(t_\mathrm{R} + t_{\mathrm{D},2} + t_\mathrm{s})^{\alpha+1} - (t_\mathrm{R} + t_{\mathrm{D},2})^{\alpha+1} - (t_{\mathrm{D},2} + t_\mathrm{s})^{\alpha+1} + t_{\mathrm{D},2}^{\alpha+1}}{t_\mathrm{R} t_\mathrm{s}} \right\}
\end{aligned} \tag{13}
$$

where we have use $t_{\mathrm{D},2}$ as abbreviation for the total delay time after a given source measurement i, $t_{\mathrm{D},2} = t_\mathrm{scan} - t_{\mathrm{D},1} - t_\mathrm{s} = t_{\mathrm{d},2} + (N - i) t_\mathrm{s}$.

The coefficient g_α giving the amplitude of the fluctuations can be determined by an Allan variance measurement (Allan 1966). The Allan variance measures in a long time series of data dumps the variance of the difference of the signal between subsequent intervals as a function of the length of these intervals. A comprehensive introduction to this technique was given by Ossenkopf (2003). The Allan variance spectrum can be computed in the same way as laid out above[2]

$$
\sigma_\mathrm{A}^2 = \frac{2 g_\alpha}{\alpha(\alpha+1)} \, 4(2^{\alpha-1} - 1) t_\mathrm{bin}^{\alpha-1} \tag{14}
$$

where t_bin denotes the length of the data intervals. This allows to express the total data uncertainty in terms of the Allan variance spectrum.

However, the fluctuations of any signal are not characterised by a single power spectrum but they consist at least of a superposition of white noise with a spectral index $\alpha = 0$ and an instrumental drift contribution with some steeper spectral index. Fortunately, we expect no correlation between the radiometric white noise and any instrumental drift, so that both the Allan variance spectrum and in the uncertainty of the calibrated data from an OTF observation are simply the sum of both contributions. The Allan variance of the white noise contribution is given by

$$
\sigma_\mathrm{A}^2 = \frac{2 \langle s(t) \rangle_t^2}{B_\mathrm{Fl} t_\mathrm{bin}} \tag{15}
$$

[2]The original definition of the Allan variance by Allan (1966) is smaller by the factor 1/2.

where B_{Fl} denotes the fluctuation bandwidth of the radiometric noise. This can be exploited to relate the coefficient g_α to this quantity. With the definition of the Allan time t_{A} as the bin size where the drift contribution and the radiometric noise contribution in the measured Allan variance spectrum show the same magnitude (Ossenkopf 2003), we can relate the radiometric noise to the coefficient g_α. We obtain the coefficient of the drift contribution as

$$g_\alpha = \frac{\alpha(\alpha+1)\langle s(t)\rangle_t^2}{4(2^{\alpha-1}-1)B_{\mathrm{Fl}}t_{\mathrm{A}}^\alpha} \tag{16}$$

Finally we can compare the total uncertainty of the calibrated data $\sigma_C^2(i)$ to the unavoidable uncertainty due to the radiometric noise in an equivalent measurement with an ideal instrument without any drifts, assuming an ideal observing mode without the need for an OFF observation. If we assume that this measurement would use the same total observing time for the N points of an OTF cycle in a given map, $t_{\mathrm{tot}} = t_{\mathrm{OFF}} + t_{\mathrm{scan}}$, the resulting data uncertainty would be

$$\sigma_{\mathrm{C,ideal}}^2 = \frac{N\langle s(t)\rangle_t^2}{B_{\mathrm{Fl}}t_{\mathrm{tot}}} \tag{17}$$

Normalising the radiometric and drift noise of the real OTF observation relative to the limiting ideal observation we obtain a measure for the actual impact of the instrumental drift on the data quality

$$\begin{aligned}
\frac{\sigma_C^2(i)}{\sigma_{\mathrm{C,ideal}}^2} \;=\; & \frac{x_{\mathrm{tot}}}{N}\Bigg\{\frac{1}{x_{\mathrm{s}}} + \frac{1-2l+2l^2}{x_{\mathrm{R}}} - \frac{2}{4(2^{\alpha-1}-1)}\Bigg[x_{\mathrm{s}}^{\alpha-1} + (1-2l+2l^2)x_{\mathrm{R}}^{\alpha-1} \\
& + (l-l^2)\frac{(2x_{\mathrm{R}}+x_{\mathrm{scan}})^{\alpha+1} - 2(x_{\mathrm{R}}+x_{\mathrm{scan}})^{\alpha+1} + x_{\mathrm{scan}}^{\alpha+1}}{x_{\mathrm{R}}^2} \\
& -(1-l)\frac{(x_{\mathrm{R}}+x_{\mathrm{D,1}}+x_{\mathrm{s}})^{\alpha+1} - (x_{\mathrm{R}}+x_{\mathrm{D,1}})^{\alpha+1} - (x_{\mathrm{D,1}}+x_{\mathrm{s}})^{\alpha+1} + x_{\mathrm{D,1}}^{\alpha+1}}{x_{\mathrm{R}}x_{\mathrm{s}}} \\
& -l\frac{(x_{\mathrm{R}}+x_{\mathrm{D,2}}+x_{\mathrm{s}})^{\alpha+1} - (x_{\mathrm{R}}+x_{\mathrm{D,2}})^{\alpha+1} - (x_{\mathrm{D,2}}+x_{\mathrm{s}})^{\alpha+1} + x_{\mathrm{D,2}}^{\alpha+1}}{x_{\mathrm{R}}x_{\mathrm{s}}}\Bigg]\Bigg\}
\end{aligned} \tag{18}$$

where we have taken all time scales relative to the Allan time t_{A}, i.e. $x_{\mathrm{tot}} = t_{\mathrm{tot}}/t_{\mathrm{A}}$, $x_{\mathrm{s}} = t_{\mathrm{s}}/t_{\mathrm{A}}$ and so on.

We find two essential contributions: the first two terms characterise the radiometric noise of the observations. This noise is higher than the radiometric noise in the ideal observation due to the x_{R}-term containing the noise from the OFF measurement. Without this term the radiometric noise ratio would be unity. All terms in the curled brackets characterise the drift contribution to the total data uncertainty. The different terms stand here for the drift occurring during the different time lags involved in the measurement. The ratio between the drift noise and the radiometric noise of the observed data can be computed by simply dividing these two contributions.

3.2 Comparison of the different calibration schemes

With Eq. (18) we can now draw quantitative conclusions on the different calibration schemes. We have computed the data uncertainty $\sigma_C^2(i)/\sigma_{\mathrm{C,ideal}}^2$ as a function of the scan length N, the spectral index of the instrumental drift α, the position of a source point within the OTF scan i, the source point integration time x_s, and the dead times between the OFF measurement and the source integrations in the scan line. To avoid too many parameters we assume as a simplification that the two dead times for moving from the source to the OFF position and vice versa are the same, $x_{d,1} = x_{d,2} = x_d$. This is well fulfilled for most observations with HIFI, due to the large inertia for the telescope but might need a small correction for fast ground-based telescopes measuring large OTF maps. Moreover, it is assumed in this section that the total integration time on the OFF position follows the standard rule $x_{OFF} = \sqrt{N} x_s$ derived for an ideal telescope (Beuther et al. 2000, Schieder & Kramer 2001).

In Fig. 5 we compare the three standard calibration schemes as discussed in Sect. 2.2. It shows the normalised total noise rms as a function of the position of a source point within the scan line for different source integration times. In the simulation a spectral index of the instrumental drift $\alpha = 2.5$ was assumed which is typical for spectroscopic fluctuations (Schieder & Kramer 2001, Ossenkopf 2003). The scan length was fixed to $N = 10$ points and the total dead time given as the sum of the dead times before and after an OFF measurement was assumed to be a quarter of the Allan time. This is a typical value that we expect for Herschel but it is somewhat too high for most ground-based telescopes.

For all three cases we find that the shortest integration time, $x_s = 0.01$ results in a relatively high noise. This can be easily understood by the low efficiency of this observation where only a small integration time is spent on the source but a large portion of the total cycle is occupied by the dead times. Because of this relatively fast cycle the noise is barely varying across the scan line. No instrumental drifts are seen. In contrast, the data from the whole scan line are dominated by instrumental drifts when the source integration time per point are in the order of the Allan time. Thus, an intermediate integration time per source point results in the lowest overall data uncertainty. In this example the optimum falls between about 0.1 Allan times for the single-OFF calibration and 0.2 Allan times for the interpolated-OFF calibration. The optimum is smaller as smaller the dead time in a scan and as higher the number of source points in a scan are.

Comparing the calibration schemes shows extreme differences in the impact of the instrumental drift. The single-OFF calibration has a huge sensitivity to instrumental drifts and the advantage of the interpolated-OFF calibration relative to the double-OFF calibration is also clearly visible. The latter has a much higher data uncertainty at the ends of the scan. In contrast, the variation of the radiometric noise from the OFF calibration in the interpolated-OFF scheme, which is visible at low integration times as small noise enhancements at the ends of the interval, is only a small contribution. In the centre of the scan double-OFF and interpolated-OFF calibration necessarily have to agree. With these results the single-OFF calibration is easily disqualified compared to the other two schemes. For all cases with many source points per OFF measurement N and with a noticeable instrumental drift, the interpolated-OFF calibration is also clearly superior to the double-OFF calibration. The latter one has advantages for short scans and small instrumental drifts.

In general the parameter study has shown that the data uncertainty due to drift effects grows with a growing spectral index of the fluctuation spectrum α and with growing dead times before and after the OFF measurements. Both parameters cannot be changed by an appropriate selection of the details of the observation or a change in the calibra-

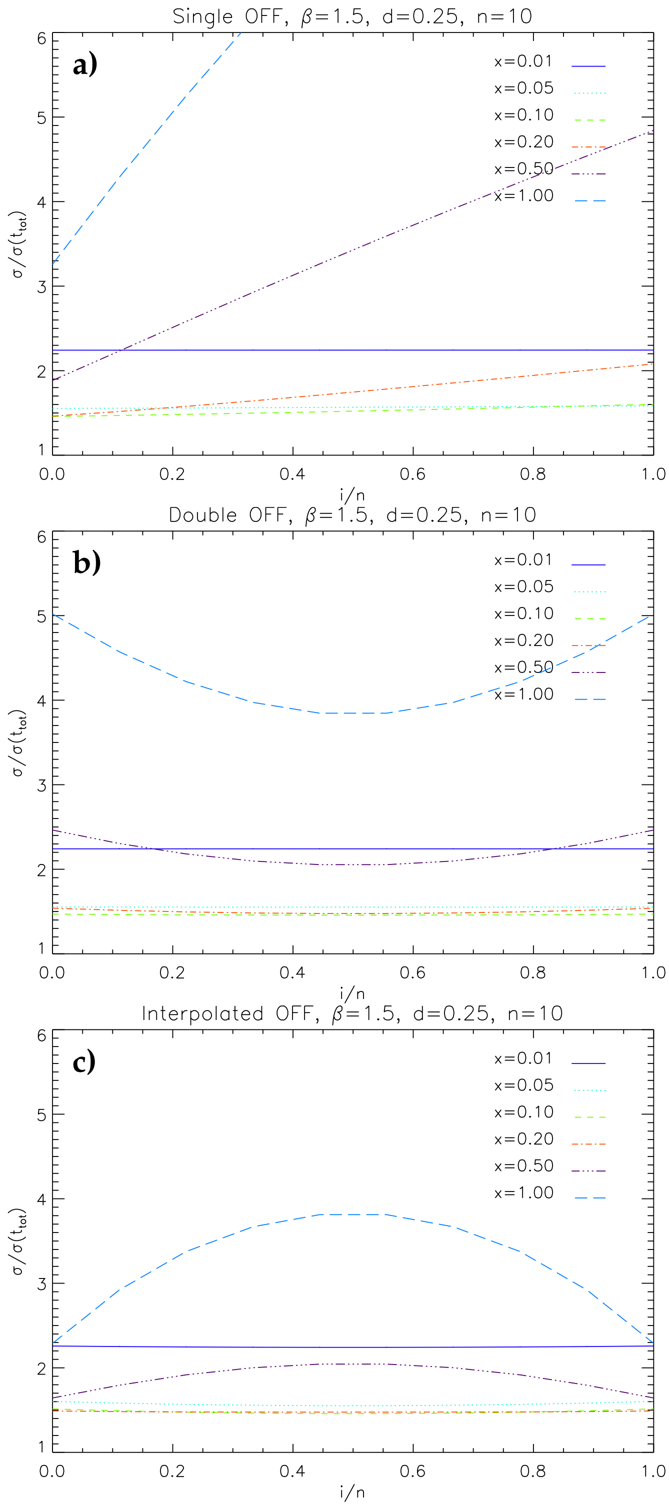

Figure 5: Variation of the total data uncertainty obtained in the different OTF calibration schemes across an OTF scan line. The rms of the fluctuations is plotted relative to the rms which would be obtained by an ideal instrument. Part **a** shows the result from the single-OFF calibration, part **b** the double-OFF calibration, and part **c** the interpolated-OFF calibration. A scan length $N = 10$, a spectral index $\alpha = 2.5$, and a total dead time $x_{\rm d,1} + x_{\rm d,2} = 0.25$ was used.

tion scheme. Thus the instrumental design should be directed towards a minimisation of both parameters. The drift uncertainty is increased by a higher number of source points in each scan but reduced in case of smaller integration times per source point. The mutual optimisation of these two parameters leads in general to the lowest uncertainties for scans with a large number of points but very short integration times. This may be limited, of course, by the size of the region to be mapped and data rate which can be taken with the instrument. A detailed optimisation taking both effects into account is given in Sect. 5.1. We have to be aware, however, that all time scales are actually relative to the Allan time. The main prerequisite for any accurate mapping observation is thus a long instrumental stability, as measured by the Allan time.

Looking at the overall pictures it is clear that the interpolated approach is in general the most robust and accurate one. In all cases where we have an accurate knowledge of the instrumental drift behaviour and where we can use very small integration times, the double-OFF calibration is, however, slightly better than the interpolation. The ideal approach would be to change the linear interpolation approach into an equivalent scheme where different portions in time from the OFF integration before and after the line are combined as into the OFF spectrum to be subtracted from the data, but this would need an arbitrarily fine granularity of the data from the OFF in time which does not seem to be practically feasible. Thus we can conclude that for telescopes which can observe really fast, like IRAM, the double-OFF approach is actually the best solution, whereas for telescopes like Herschel with long delay times and a limited data rate we should rather use the interpolation which is only slightly worse for small integration times but much better in case of a slow timing.

4 Application to observed data

The different calibration schemes were tested using existing molecular line mapping observations performed with the KOSMA 3 m telescope. An arbitrary OTF patch was taken from a larger W 75 survey in ^{13}CO 2-1 obtained by Jakob et al. (in prep.). The observations were taken in the ordinary OTF mode where after each line of the patch, containing 20 source integrations of 5 s, one OFF integration of 23 s, corresponding to $\sqrt{20} \times 5$ s, was performed. For the slew from the end of an OTF scan to the OFF position a dead time of 19 s was needed, the slew from the OFF position to the beginning of the subsequent OTF scan took 12 s. The spectral resolution of the used backend is 360 kHz and the corresponding fluctuation bandwidth 560 kHz. The spectroscopic Allan time of the instrument at this resolution is about 120 s. The Allan time of the whole system including the atmosphere is estimated to be approximately 80 s. The drift index of the fluctuations falls between 2 and 3. For all computations we assume 2.5 here. The single-sideband system temperature during the observations was about 350 K.

To emphasise the drift effects we first consider maps of line integrated intensities, where the full velocity range of the ^{13}CO line from 4 to 8 km/s was integrated corresponding to an effective bin width of 2.9 MHz. When the bin width exceeds the fluctuation bandwidth of the single channels considerably the effective profile is close to a box car profile, so that the resulting fluctuation bandwidth is equal to the bin width. The effective Allan time at this width is then $t_{\rm A} = (560\ \mathrm{kHz}/2.9\ \mathrm{MHz})^{1/2.5} \times 80\ \mathrm{s} \approx 40\ \mathrm{s}$ (Schieder & Kramer 2001) so that one OTF cycle corresponds to approximately 4 Allan times at this resolution. Thus we expect that drift effects start to become noticeable above the radiometric noise level in the integrated maps.

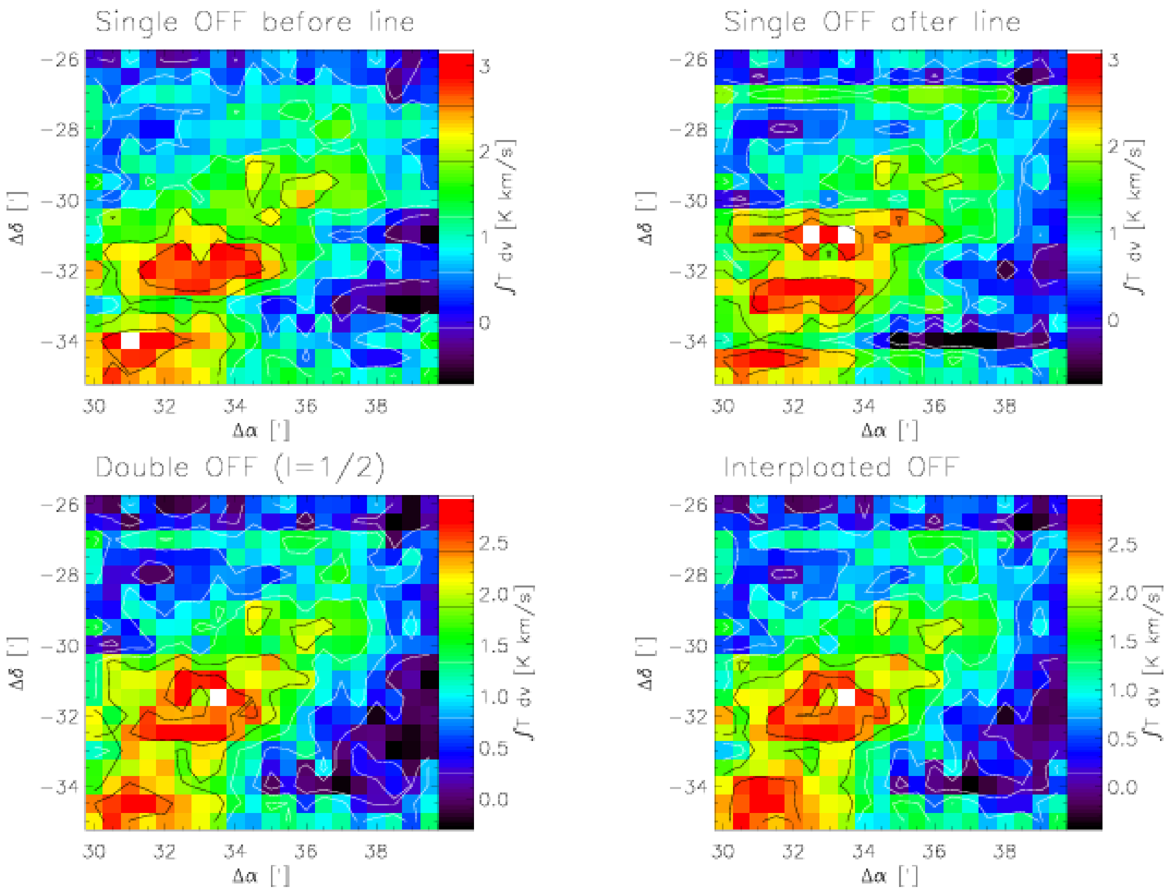

Figure 6: Demonstration of the influence of the different calibration schemes on the appearance of the produced line maps. The maps in the upper panels were obtained when calibrating with the single OFF measurement before and after each line. The lower left panel shows the result with a fixed sum from the two adjacent OFF measurements ($l = 1/2$) and the lower right panel shows the result when using a time interpolation between both OFF measurements. The map was measured in horizontal stripes. After each line an OFF measurement was taken.

Fig. 6 compares the four integrated line maps obtained in the different calibration schemes. First we see immediately that the two single-OFF calibration maps show a very "stripy" structure. This is more prominent when using the OFF after the scan lines than with the OFF before the line but also in this first case one can clearly notice several elongated structures in horizontal direction which are only drift artifacts and not real structures. The stripes are not restricted to one end of the scans but cover large parts of the map. In contrast, the maps obtained from the double-OFF calibration and the interpolated-OFF calibration appear basically isotropic and they are very similar. The small remainders of a stripy structure at the third and eleventh line from the top in the double-OFF map are, however, further suppressed when using the interpolated-OFF integration. We can conclude that the first application of the different calibration schemes to real observations proves already the theoretical considerations that the single-OFF calibration is clearly more susceptible to drift effects than the other calibration schemes so that it should be avoided. The interpolated-OFF calibration seems to be slightly better than the double-OF calibration but this is hardly significant in this example.

From Eq. (18) we can actually compute the drift noise that we expect in the different calibration schemes. The ideal observation would result in a radiometric noise of $\sigma \approx 0.1$ K. When calibrating the data following the single-OFF scheme, the actual radiometric noise is higher by the factor 1.87. From Fig. 5 we see that the maximum drift occurs at the source point with the maximum temporal distance to the corresponding OFF measurement. When using the OFF measurement before each scan for calibration we find that the maximum drift noise $\sigma^2_{\rm C,drift} = 2.4\sigma_{\rm C,ideal} = 1.3\sigma_{\rm C,rad.}$. With the OFF measurement after each scan we arrive at somewhat higher values of $1.4\sigma_{\rm C,rad.}$ due to the slightly longer slew time at the end of each scan. It is clear that these drift effects are visible as global structures in the integrated line maps, but for each single source point they can still be hidden in the radiometric noise. For the double-OFF calibration the radiometric noise is somewhat smaller, $\sigma_{\rm C,rad.} = 1.71\sigma_{\rm C,ideal}$, because of the lower noise from the OFF data including two OFF measurements. The maximum drift error is expected at the ends of the scan interval (see Fig. 5). We obtain $\sigma^2_{\rm C,drift} = 0.56\sigma_{\rm C,ideal} = 0.33\sigma_{\rm C,rad.}$. Thus, the double-OFF integration should already remove all visible drift effects from the maps. For the interpolated-OFF calibration the maximum drift error occurs again in the centre of a scan line. Here, we find $\sigma^2_{\rm C,drift} = 0.35\sigma_{\rm C,ideal} = 0.2\sigma_{\rm C,rad.}$ with the same radiometric noise as in the double-OFF calibration. Towards the ends of the OTF scan the radiometric noise grows slightly up to $1.78\sigma_{\rm C,ideal}$ but the drift noise decreases further down to $\sigma^2_{\rm C,drift} = 0.14\sigma_{\rm C,ideal} = 0.08\sigma_{\rm C,rad.}$. Thus all drift effects should be completely suppressed in the integrated line map when applying the interpolated-OFF calibration.

We have to keep in mind, however, that the Allan variance is only a statistical measure to characterise the drift behaviour. Thus we cannot expect to find uniform drift effects in all scans but we will always find lines with stronger and weaker indications of instabilities. This is well visible in Fig. 6. Eq. (18) is strictly valid only for the ensemble average over many observations. The possible spread of the actual drift noise in a particular observation relative to this average value grows towards higher spectral indices of the fluctuations. When interpreting calibrated data, one thus has always to take into account that the errors computed here are no error limits but 1σ values of a stochastic process.

So far we have concentrated on the drift effects which are best visible in the integrated line maps. To study the effect of correlated noise we have to use single channels instead where the radiometric noise is larger and the drift effects are smaller. For a single channel an ideal observation would give a radiometric noise of $\sigma \approx 0.23$ K and the Allan time is about 80 s. Fig. 7 shows the maps of the single spectrometer channel at the position of the peak of the average line profile obtained from the different calibration schemes. Here we find, much smaller differences between the calibration schemes than in Fig. 6 but it still seems that these differences are dominated by the drift effects and not by the different introduction of correlated noise. This can be seen by comparing the two figures. We find that those lines showing drift signatures in the integrated maps are the same lines that show the smaller deviations in the channel maps although the radiometric noise is higher in the channel maps.

This is in agreement with the results that we get from Eq. (18). The amount of correlated radiometric noise relative to the ideal observation is the same as for the integrated map discussed above. Thus we have about 25 % more noise from the OFF positions in

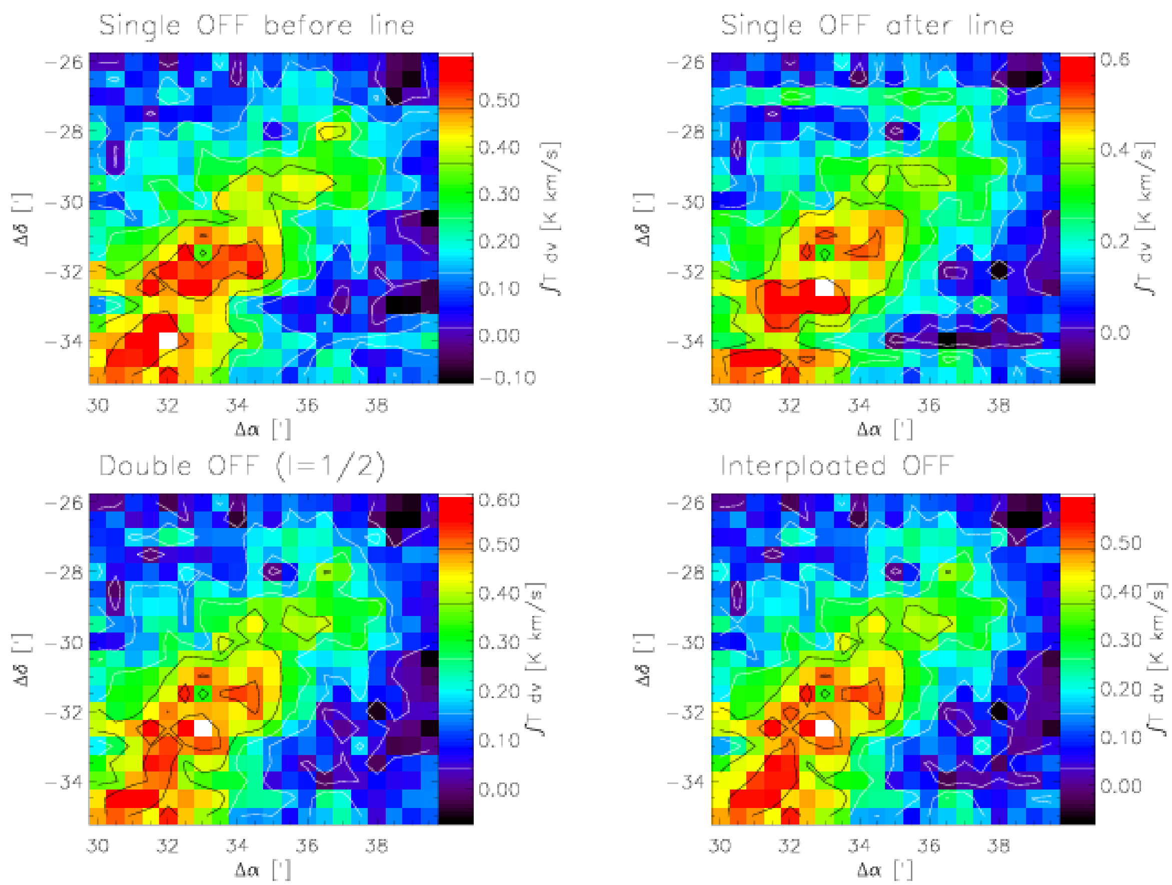

Figure 7: Channel map at 5.7 km/s obtained in the different calibration schemes from the same data as used for the integrated line maps in Fig. 6.

the single-OFF calibration and about 10 % more noise at the edges of the interpolated-OFF calibration than in the double-OFF calibration but this is not noticeable by eye in the figure. Thus we can conclude that for maps with more that 10 pixels the introduction of correlated noise by the different calibration schemes is sufficiently similar so that they should be chosen basically on their capability of correcting the drift of the system and not on differences in the correlated radiometric noise. Thus we restrict ourselves to the interpolated-OFF calibration in the following.

5 Global optimisation

5.1 Minimisation of the total noise

Aside from identifying the optimum calibration scheme for OTF observations, the formalism introduced in Sect. 2 can also be used to optimise the actual timing of the observations. In Sect. 2.3 it was discussed already that it is possible to adjust the time spent for the OFF integration by considering the correlated noise and the resulting total data uncertainty. Moreover, Fig. 5 has shown that it is possible to compute the drift noise as a function of the source integration time. Consequently, we can try to adapt the scanning speed of the OTF observations to provide source integration times resulting in a minimum uncertainty of the calibrated data.

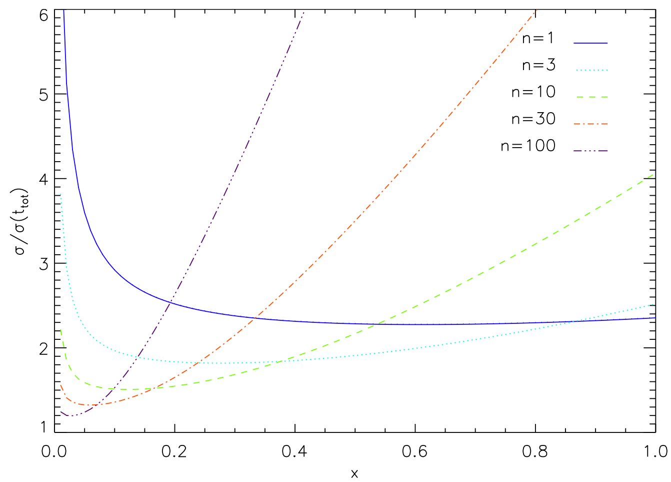

Figure 8: Relative rms of the total data uncertainty from radiometric and drift noise obtained in the interpolated-OFF calibration as a function of the source point integration time relative to the Allan time for different scan lengths. A spectral index $\alpha = 2.5$, and a dead time $2x_\mathrm{d} = 0.25$ was used here.

This is demonstrated in Fig. 8 where the resulting data uncertainty is plotted as a function of the source integration time for different scan lengths. A spectral index $\alpha = 2.5$ typical for spectroscopic drifts and a total dead time of 0.25 Allan times were used here. The plot shows the maximum value across the OTF scans, which is typically reached at the ends of the scan for short cycles and in the centre as soon as drift effects start to dominate.

For all scan lengths we find a characteristic minimum corresponding to the optimum source integration time. When using longer integration times the drift effects start to dominate. At smaller integration times the relative overhead from the dead times for slewing to and from the OFF position makes the observations inefficient so that the radiometric noise too high. We also see that the relative accuracy of the observations at the optimum timing grows towards more source points within each OTF scan. The equivalent plot for the double-OFF calibration shows a steeper increase of the noise when the source point integration time is above its optimum value but minima which are slightly deeper than the minima shown here.

A special behaviour occurs for very shallow spectra. There, the slope at large integration times is the same for all scan lengths and we find no intersection of the curves. This means that very long scans are always favourable even if the resulting cycle length is much larger than the Allan time. This can be easily understood from the fact that in fluctuation spectra shallower than $1/f$ the noise is still reduced with increasing integration time, just like in the familiar case of white noise, but with another slope. The exact value for the transition to this behaviour depends on the dead times involved but it occurs usually for $\alpha < 0.75$.

Independent from the spectral index of the fluctuations we find that the best observing mode is always given by very long scans with many points and a very short integration time per point in each scan. A full observation is then obtained from many of these short-time coverages. This was shown already by Schieder & Kramer (2001). Unfortunately, there are practical limitations to this approach in each instrument. A telescope cannot move arbitrarily fast and the integrated data cannot be read out and dumped at an infinite data rate. Thus, the minimum relative integration time x_{min} set by the instrument is a limiting quantity for the optimum OTF timing. Moreover, the size of the astronomical source never justifies an arbitrarily large map, so that the maximum number of source points is also constrained. Taking these two limitations a plot like Fig. 8 computed for the actual slewing time can then be used to obtain the optimum observing mode. In most cases, the solution will still fall at the extreme provided by the maximum possible number of points and the minimum possible integration time.

The OTF mode implemented at most ground-based telescopes always identifies the OTF scan length with the length of a single row in an OTF map. However, there is no a priori requirement for this identity. Thus the observing mode definition of OTF modes for the Herschel Space Telescope foresee also to use only parts of map rows or multiple rows within one OTF scan between two OFF measurements. This is partially motivated by the relatively slow slew to the OFF position exceeding the turn time between subsequent lines in an OTF mapping. In case of such an inequality between the scan length N and the length of a map row N_{row} the additional turn delays t_{turn} between subsequent rows have to be taken into account when computing the total noise in the data. For a point i measured within an OTF scan of length N, the number of turns before and after this point are $N_{\mathrm{turn,1}} = (i-1)/N_{\mathrm{row}}$ and $N_{\mathrm{turn,2}} = (N-i)/N_{\mathrm{row}}$, respectively. Hence, the total delay before the measurement $x_{\mathrm{D,1}}$ has to be increased by $N_{\mathrm{turn,1}} x_{\mathrm{turn}}$, the total delay after the measurement $x_{\mathrm{D,2}}$ by $N_{\mathrm{turn,2}} x_{\mathrm{turn}}$ and the total scan length x_{scan} by $(N_{\mathrm{turn,1}} + N_{\mathrm{turn,2}}) x_{\mathrm{turn}}$ in Eq. (18), where x_{turn} denotes the turn time relative to the Allan time, $x_{\mathrm{turn}} = t_{\mathrm{turn}}/t_{\mathrm{A}}$.

In this case, the minimum relative data uncertainty is no longer provided by the maximum scan length and the minimum possible integration time because of the increasing overhead for turns when increasing the scan length. The optimisation has to be done by actually evaluating Eq. (18) for different scan lengths and integration times. This is demonstrated in Fig. 9 showing the total noise rms as a function of the source integration time and the scan length for a map where the row length is restricted to 30 points and the relative turn time is $x_{\mathrm{turn}} = 0.15$.

The most important feature in this plot is the large length of the valley in terms of the scan length, but to a lesser extend also its width in terms of the source integration time. The 2 %-contour encloses already a factor six in scan length and a factor two in the integration time The whole plotted 10 % range is even much larger. This means that OTF observations are extremely robust with respect to bad timings. Even when using setups which are very different from the optimum the noise rms is typically only enhanced by a few up to some ten percent. This explains why the OTF mode is used very successfully at many ground-based telescopes without a thorough theoretical analysis.

The staircase structure of the contours reflects additional turns which are required when the scan length exceeds multiples of the row length. There are several minima with their deepest points always at integer multiples of the row length. In this example, the optimum scan length falls at 120 points, but scans with 150, 180 or 210 points and a slightly shorter integration time are practically not worse. The optimum source integration time is no longer determined by the minimum time allowed by the instrument but still short compared to the Allan time. In numerous tests with parameters typical

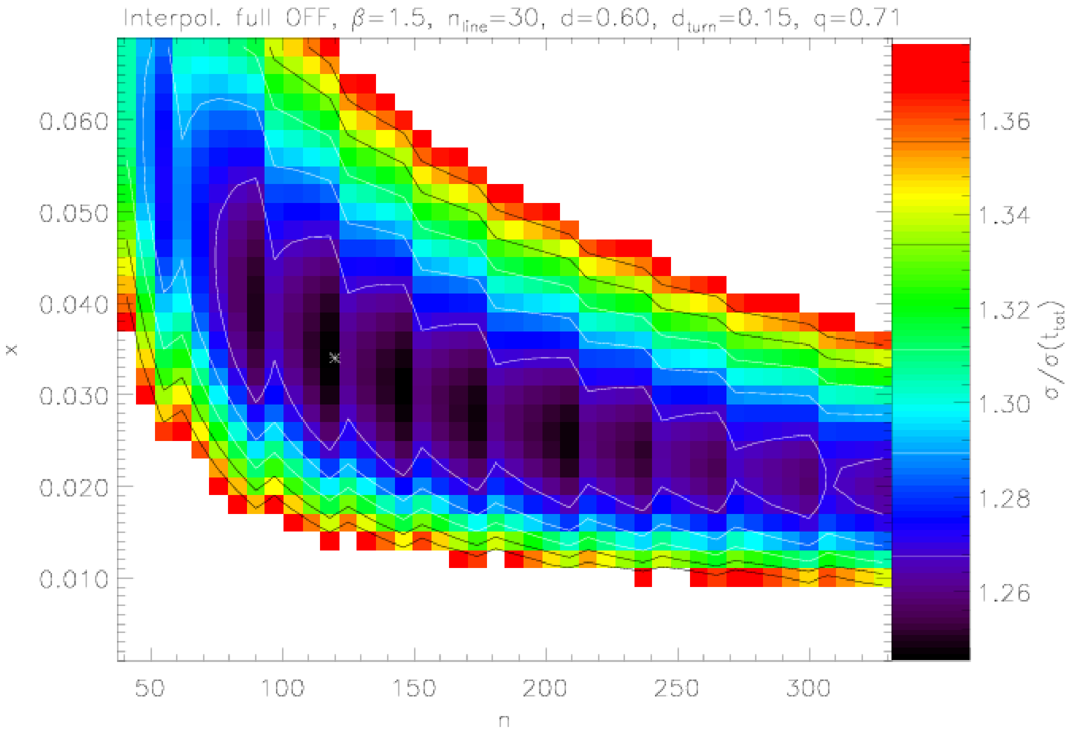

Figure 9: Relative rms of the calibrated data in OTF observations as a function of the scan length and the integration time per source point relative to the system Allan time. Values of more than 10 % above the minimum are clipped in the plot. The asterisk marks the optimum setup resulting in the minimum noise. A row length of 30 points, an OFF dead time $2x_{\rm d} = 0.6$, a turn time of the telescope $x_{\rm turn} = 0.15$, and a spectral index $\alpha = 2.5$ were used here.

for different telescopes we found no case with a minimum not corresponding to a full row. Thus we can always complete rows in an OTF scan before going to the OFF position. However, it is also typical that one can combine several rows in an OTF scan. As the topology of the surface plotted in Fig. 9 is relatively simple, an optimisation of OTF observations based on Eq. (18) is always possible without much computational effort even if there is no analytic expression for the optimum timing.

Eq. (18) can also be used to check the optimum integration time for the OFF measurement. In Sect. 2.3 qualitative arguments had shown that for the interpolated-OFF calibration scheme an OFF integration time of $t_{\rm OFF} = 2/3 \times \sqrt{N} t_{\rm s}$ should be sufficient. By introducing q as a free parameter characterising the relative OFF integration time $t_{\rm OFF} = q\sqrt{N} t_{\rm s}$ we can directly compute the impact of this parameter on the total noise of the calibrated data. The result is shown in Fig. 10. Here, we have determined the global minimum of the total noise error depending on the scan length, the q parameter and the source integration time. As discussed above the minimum falls at the shortest possible integration time when no restrictions are made to the scan length. Thus this parameter is not plotted here, but only the dependency of the noise on the other two parameters.

We find again a very broad range of good parameters. At the optimum scan length of 150 points, the 2 %-contour covers q values between 0.4 and 1.6. Thus, the exact choice of the OFF time has hardly any influence on the total data uncertainty of the calibrated

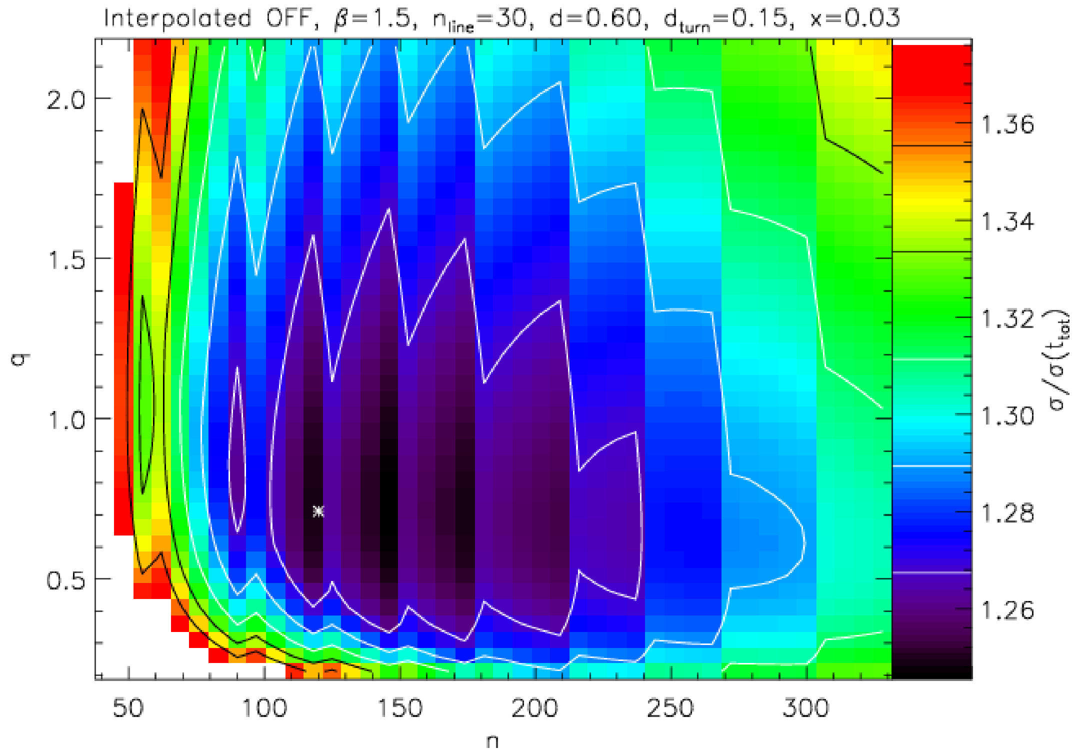

Figure 10: Relative rms of the calibrated data in OTF observations as a function of the scan length and the q parameter determining the OFF integration time. The parameters from Fig. 9 were used together with the optimum source integration time of $x_s = 0.03$ given there.

data. We find the same robustness discussed above for the scan lengths. Varying the model parameters showed that the optimum scan length depends strongly on the minimum allowed integration time and the spectral index of the fluctuations but that the optimum q-parameter is always close to 0.7. like in Fig. 10. Thus this value can be used for all observations applying the interpolated-OFF calibration scheme discussed in Sect. 2.3.

5.2 Examples

To provide a feeling for the results discussed they will be applied to a few realistic examples. Ground based telescopes have the general advantage that they can quickly slew to the off position and store the measured data at a high rate. In principle, they could also perform a fast turn between subsequent rows in a map, but this feature is rarely implemented. Their big disadvantage is the atmospheric instability. A typical Allan variance spectrum measured in the 345 GHz window in good weather conditions at the KOSMA telescope shows an Allan time of about 80 s and a spectral index $\alpha \approx 2.5$ for spectroscopic measurements with a fluctuation bandwidth of 1.6 MHz corresponding to a backend velocity resolution of about 1 km/s. In contrast, the continuum drifts at the same resolution show an Allan time of about 8 s and a shallow spectrum with an index of about $\alpha \approx 1.5$.

Assuming a map size of at most 30 points, a minimum data taking interval of 1 s, a dead time for slewing to the OFF position of 10 s, and a dead time for a turn between the rows of 8 s we find that for spectroscopic observations (subtracting a zero-order baseline) the optimum scan consists of 180 points, i.e. six rows, observed with an integration time of 2 s per source point. The full range of good observing parameters covers scan lengths between 120 and 270 points and integration times between 1 s and 4 s. The drift contribution to the total noise is only 8 % of the radiometric noise at the optimum timing. If the instrument is not capable to observe subsequent rows without much delay, so that the scan lengths are restricted to the row length, the optimum integration time is 6 s and the total rms of the data is increased by 5 % relative to a telescope with an implemented turn. For continuum observations the optimum integration time is the minimum allowed integration time, the optimum scan length is 60 points but the relative drift contribution is already 70 %. In this case, the restriction of the scan length to the row length provides almost no deterioration of the observing efficiency, in fact by reducing the scan length to one row, the total noise rms is increased only by 1 % but the drift contribution relative to the radiometric noise drops to 51 %.

For HIFI observations with the Herschel Space Telescope we expect a more stable configuration, with an Allan time of about 150 s for spectroscopic drifts at a fluctuation bandwidth of 1.6 MHz. The drift index should also be close to $\alpha = 2.5$. On the other hand, all telescope slews are relatively slow so that we can estimate a slewing time of about 40 s when going to an OFF position which is 20′ apart from the source and a turn time of about 20 s. Moreover, the used hot electron mobility transistors are known to dominate the fluctuation spectrum for continuum measurements resulting in an Allan time of about 1.5 s and a spectral shape somewhat shallower than $1/f$ noise at the same spectral resolution. The minimum data taking interval will be 1 s for all mapping observations. For line maps the optimum scan length is 180 points. All integer multiples of 30 between 90 and 270 are almost as good. The optimum integration time falls between 2 s and 8 s with the exact minimum at 4 s. The drift noise contribution at the optimum parameters is 10 % of the radiometric noise. Here, the complexity of scanning subsequent rows in opposite directions is well justified because a limitation of the scan length to the row length would increase the noise rms obtained in the same observing time by 9% corresponding to a 19% loss of observing efficiency. Continuum observations in OTF mode always have to use the fastest data rate available and restrict themselves to one row but the drift noise in this setup would exceed the radiometric noise already by a factor 2.4. Thus, we have to conclude that continuum observations with HIFI cannot be performed in the OTF mode with a reasonable accuracy.

5.3 Discussion

OTF observations in general and the optimisation scheme proposed above in particular have a serious drawback. When reusing the calibrated data for purposes which were not foreseen when planning the observations, by spatially integrating over several points or by combining neighbouring pixels in the spectra, the relative gain in the noise reduction is always lower than for pure radiometric noise.

The effect is well known for spatial rebinning. When maps taken in OTF mode a rebinned to a coarser resolution the contribution of the correlated noise from the OFF position stays constant (Beuther et al. 2000). By extending OTF scans over several rows of a map this effect is in principle even more enhanced. On the other hand, the total noise contribution from the OFF measurement drops with increased scan lengths so that the effect of correlated noise is also somewhat reduced by extending the scans. With the proposed optimisation scheme the same becomes also true for the spectral rebinning. The Allan time used to optimise the observations is determined by the ratio of drift noise and radiometric noise. Rebinning of the spectra to a coarser resolution only reduces the radiometric noise so that the relative contribution of the drift noise is enhanced.

Thus, the value of OTF maps with respect to their reuse for binning either spatially of spectroscopically is always limited. In both cases artificial structures due to instrumental drifts or due to the correlated noise are enhanced. Consequently, a very careful planning of the observations has to be performed. The observer has to find a compromise between the efficiency of the observations and their re-usability. The optimisation scheme should always be applied at the level of the coarsest spatial and spectral resolution that might be used for interpreting the calibrated data. Thus the planning can well start from a spatial grid that is not fully sampled even if the observations will be taken on a Nyquist sampled grid. This guarantees that all artifacts from the observing mode are suppressed, however, at the costs of the observing efficiency. As more precise the scientific application of the measured data can be specified in terms of spatial and spectroscopic resolution as better can the actual observing scheme be adapted to the application resulting in more efficient observations.

Moreover, we have to introduce a general warning. The optimum total cycle times for the OTF observations derived here can easily exceed the Allan stability time of the instrument by a large factor. This is a major difference to the behaviour of single-point ON-OFF observations where reasonable maximum cycle times are in the order of 2–3 Allan stability time scales. All conclusions were drawn here on the assumption that the fluctuation spectrum follows a simple power law. Whereas it is justified to fit almost every spectrum over a dynamic range of about three by a power law within the accuracy of the method this is no longer guaranteed over a much larger scale. Thus the Allan variance spectrum has to be determined over at least the time scale expected for the longest OTF observing cycles and not only over a few Allan times. Only if this long term spectrum is well fitted by a power law the formalism derived here can be applied using the corresponding spectral index of the fluctuations α.

6 Conclusions

In most cases mapping observations should follow the scheme known from OTF maps where the calibration of several source points uses a common OFF measurement for reference. This is in general far more efficient than all other reference modes. It introduces, however, correlated noise across the calibrated map stemming from the common OFF integration. The total amount of correlated noise grows with the square root of the number of points in a scan between two OFF measurements. To minimise the impact of this correlated noise the two neighbouring OFF measurements should always be used for the calibration. Their optimum integration time is approximately $0.7\sqrt{N}t_{\mathrm{s}}$.

In most cases the calibration of the source data should follow the interpolated-OFF scheme where the data from both neighbouring OFF measurements are weighted according to their temporal distance from the source measurement. This compensates all linear drifts of the instrument and results in the lowest total uncertainty of the calibrated data. The single-OFF calibration still used at several telescopes should be immediately abandoned because of the strong sensitivity of the calibrated data to drift effects. For very short scans with less than 10 points at a fast telescope the double-OFF calibration is superior to the interpolated-OFF calibration but its use is limited to these cases.

The total uncertainty of the calibrated data consisting of radiometric noise and drift noise can be computed when the fluctuation spectrum of instrumental instabilities is known, i.e. an Allan variance measurement was performed. The result can be used to optimise the time line for the actual realization of the mapping observations. It turns out that the OTF observing mode is in general very robust with respect to non-optimal timings. The scan length and the source integration time can be varied within a relatively broad range without increasing the total noise in the calibrated data by more than a few percent.

The optimisation reveals some general relations on conditions for accurate and efficient mapping observations:

- The efficiency of all mapping modes grows with growing map size.
- The possibility of fast data readouts is in many cases essential to minimise the drift contributions.
- In most conditions OTF scans can consist of integer multiples of complete map rows.

We have to stress again that the most essential impact on the data accuracy is provided by the system stability. All time scales have to be considered relative to the Allan time. The main prerequisite for any accurate mapping observation is thus a long instrumental stability, as measured by the Allan time. Due to the low gain stability of most heterodyne instruments it turns out that it is practically impossible to derive significant information on the continuum level of astronomical sources using the mapping modes discussed here. They are always heavily influenced by the instrumental drifts.

Both the general design of the mapping modes with a common OFF measurement and the optimisation scheme proposed limit the re-usability of the data in terms of spatial or spectroscopic rebinning. The setup should be optimised with a clear picture of the resolution requirements set by the scientific goal of an observation.

Acknowledgements

I want to thank Rudolf Schieder and Michel Perault for useful discussions. The research has made use of NASA's Astrophysics Data System Abstract Service.

A Raster map observations

Raster map observations differ from the OTF observations discussed in the main part of this paper by two properties. First, the effective beam of the observation is always equal to the actual telescope beam. It does not suffer from the beam broadening discussed for OTF maps in Sect. 2.1. This advantage is, however, mostly compensated by the disadvantage of the dead time between different points of a map. The observation of each source point is characterised by two time constants here, the source integration time t_s and the slew time to the next map position t_m. For all points in the map, except for the last point of a scan, the total time needed for the measurement is given by $t_{\mathrm{s,tot}} = t_\mathrm{s} + t_\mathrm{m}$. No additional turn time between two map rows is required. If we redefine the slew time to the OFF position as $t'_{\mathrm{d},2} = t_{\mathrm{d},2} - t_\mathrm{m}$ we can use all equations derived above for the calibration and the noise estimate in the OTF mode by using t_s whenever the integration time counts and $t_{\mathrm{s,tot}}$ whenever delays enter.

In particular the interpolation measure l derived in Sect. 2.2 (Eq. 3) turns into

$$l = \frac{t_\mathrm{R}/2 + t_{\mathrm{d},1} + (i-1/2)t_{\mathrm{s,tot}}}{t_\mathrm{R} + t_{\mathrm{d},1} + t'_{\mathrm{d},2} + N t_{\mathrm{s,tot}}} \tag{19}$$

For the estimate of the total noise in the data Eq. (18) can still be used when the total delays include the additional slew times, i.e.

$$\begin{aligned} x_{\mathrm{D},1} &= x_{\mathrm{d},1} + (i-1)x_{\mathrm{s,tot}} \\ x_{\mathrm{D},2} &= x_{\mathrm{d},2} + (N-i)x_{\mathrm{s,tot}} = x'_{\mathrm{d},2} + (N-i)x_{\mathrm{s,tot}} + x_\mathrm{m} \\ x_{\mathrm{scan}} &= x_{\mathrm{d},1} + N x_{\mathrm{s,tot}} + x'_{\mathrm{d},2} \end{aligned} \tag{20}$$

The resulting general behaviour corresponds to an OTF map with very long delays before and after the lines. The corresponding optimum timing may consist of scan lengths which are shorter than the row lengths but there are no qualitative differences to the properties discussed for OTF observations.

References

Allan D.W. 1966, Proc. IEEE 54, no. 2, 221

Ball J.A. 1976, in Meeks M. (ed.): Methods of Experimental Physics, Vol. 12, Astrophysics, Part C, Radio Observations, Acad. Press, p. 55

Bensch F., Stutzki J., & Ossenkopf V. 2001, A&A 366, 636

Beuther H., Kramer C., Deiss B., Stutzki J. 2000, "CO mapping and multi-line-analysis of Cepheus B", A&A 362, 1109

Kutner M.L., Ulich B.L. 1981, ApJ 250, 341

Ossenkopf V., 2002, "The HIFI intensity calibration framework", ALMA-Memo 442

Ossenkopf V., 2003, "A unified Allan variance computation scheme", ICC/2003-013, 07/31/03

Roelfsema P. et al. 2002, "HIFI Calibration Use Cases", ICC/2001-005, 02/20/02

Schieder R., Rau G., Vowinkel B. 1985, in Instrumentation for Submillimetrer Spectroscopy, ed. E. Kollberg (Academic Press), 189

Schieder R., Kramer C. 2001, A&A 373, 746

Schieder R., Tolls V., Winnewisser G. 1998, Experimental Astronomy 1, no. 2, 101

Whyborn N.D. 2003, DM IF-1 Amplifier Gain Stability Summary, SRON Technical Note 06/02/2003